Pilot Comparison of ^{68}Ga-RM2 PET and ^{68}Ga-PSMA-11 PET in Patients with Biochemically Recurrent Prostate Cancer

Ryogo Minamimoto[1,2], Steven Hancock[3], Bernadette Schneider[2], Frederick T. Chin[2], Mehran Jamali[1,2], Andreas Loening[4], Shreyas Vasanawala[4], Sanjiv Sam Gambhir[2], and Andrei Iagaru[1]

[1]Division of Nuclear Medicine and Molecular Imaging, Department of Radiology, Stanford University, Stanford, California; [2]Molecular Imaging Program at Stanford, Department of Radiology, Stanford University, Stanford, California; [3]Department of Radiation Oncology, Stanford University, Stanford, California; and [4]Department of Radiology, Stanford University, Stanford, California

Glu-NH-CO-NH-Lys-(Ahx)-[^{68}Ga(HBED-CC)] (^{68}Ga-PSMA-11) is a PET tracer that can detect prostate cancer relapses and metastases by binding to the extracellular domain of PSMA. ^{68}Ga-labeled DOTA-4-amino-1-carboxymethyl-piperidine-D-Phe-Gln-Trp-Ala-Val-Gly-His-Sta-Leu-NH2 (^{68}Ga-RM2) is a synthetic bombesin receptor antagonist that targets gastrin-releasing peptide receptors. We present pilot data on the biodistribution of these PET tracers in a small cohort of patients with biochemically recurrent prostate cancer. **Methods:** Seven men (mean age ± SD, 74.3 ± 5.9 y) with biochemically recurrent prostate cancer underwent both ^{68}Ga-PSMA-11 PET/CT and ^{68}Ga-RM2 PET/MRI scans. SUV_{max} and SUV_{mean} were recorded for normal tissues and areas of uptake outside the expected physiologic biodistribution. **Results:** All patients had a rising level of prostate-specific antigen (mean ± SD, 13.5 ± 11.5) and noncontributory results on conventional imaging. ^{68}Ga-PSMA-11 had the highest physiologic uptake in the salivary glands and small bowel, with hepatobiliary and renal clearance noted, whereas ^{68}Ga-RM2 had the highest physiologic uptake in the pancreas, with renal clearance noted. Uptake outside the expected physiologic biodistribution did not significantly differ between ^{68}Ga-PSMA-11 and ^{68}Ga-RM2; however, ^{68}Ga-PSMA-11 localized in a lymph node and seminal vesicle in a patient with no abnormal ^{68}Ga-RM2 uptake. Abdominal periaortic lymph nodes were more easily visualized by ^{68}Ga-RM2 in two patients because of lack of interference by radioactivity in the small intestine. **Conclusion:** ^{68}Ga-PSMA-11 and ^{68}Ga-RM2 had distinct biodistributions in this small cohort of patients with biochemically recurrent prostate cancer. Additional work is needed to understand the expression of PSMA and gastrin-releasing peptide receptors in different types of prostate cancer.

Key Words: prostate cancer; ^{68}Ga; RM2; PSMA; PET/MRI; PET/CT

J Nucl Med 2016; 57:557–562
DOI: 10.2967/jnumed.115.168393

Prostate cancer recurrence has been assessed by measurement of prostate-specific antigen (PSA) levels and velocity. A detectable or rising PSA level after therapy is considered to indicate biochemical recurrence, or "PSA failure," even when there are no symptoms or signs of locally recurrent or metastatic disease (*1,2*). By enabling selection of appropriate treatment, such as local salvage therapy or systemic therapy, imaging is useful for identifying locally recurrent or distant lesions when the PSA level is rising (*3*).

Conventional imaging techniques such as ultrasound, contrast-enhanced CT, and MRI have limited sensitivity and specificity for local recurrence and metastatic lesions (*3*). ^{11}C-acetate, ^{11}C-choline, and ^{18}F-choline have been reported to be useful for the diagnosis of recurrent or metastatic prostate cancer (*4–8*). However, the very short half-life of ^{11}C limits its use to facilities equipped with a cyclotron. Although choline-based PET/CT is widely used outside the United States for imaging prostate cancer, numerous studies have reported a low sensitivity and specificity for this technique, especially at low PSA levels (*9,10*).

Prostate-specific membrane antigen (PSMA) is significantly overexpressed in prostate cancer cells in comparison with other PSMA-expressing tissues, such as kidney, proximal small intestine, and salivary glands (*11*), and therefore provides a promising target for prostate cancer–specific imaging (*12*). After initial reports of a ^{124}I/^{131}I-labeled small molecule targeting PSMA for prostate cancer therapy (*13*), methods have recently been developed to label PSMA ligands with both ^{68}Ga and ^{177}Lu, enabling their use for theranostics (*14,15*). Initial experience with PET/CT using Glu-NH-CO-NH-Lys-(Ahx)-[^{68}Ga(HBED-CC)] (^{68}Ga-PSMA-11) suggests that this novel tracer can detect prostate cancer relapses and metastases with high contrast by binding to the extracellular domain of PSMA, followed by internalization (*16*).

^{68}Ga-labeled DOTA-4-amino-1-carboxymethyl-piperidine-D-Phe-Gln-Trp-Ala-Val-Gly-His-Sta-Leu-NH2 (^{68}Ga-RM2, or ^{68}Ga-DOTA-bombesin, formerly also known as BAY86-7548) is a synthetic bombesin receptor antagonist that targets gastrin-releasing peptide receptors (*17*). Gastrin-releasing peptide receptor proteins are highly overexpressed in several human tumors, including prostate cancer (*18*), and gastrin-releasing peptide receptor has been detected in 63%–100% of human prostate cancer tissue (*19,20*). Because ^{68}Ga-RM2 and ^{68}Ga-PSMA-11 target different biologic processes, understanding how these two tracers behave in patients with biochemically recurrent prostate cancer is critical to finding the best management options for this clinical scenario.

The aim of this study was to compare the biodistribution of ^{68}Ga-RM2 and ^{68}Ga-PSMA-11 in patients with biochemically recurrent prostate cancer and to compare uptake of ^{68}Ga-PSMA-11

Received Oct. 17, 2015; revision accepted Nov. 18, 2015.
For correspondence or reprints contact: Andrei Iagaru, Division of Nuclear Medicine and Molecular Imaging, Department of Radiology, Stanford University, 300 Pasteur Dr., C21, Stanford, CA 94305-5281.
E-mail: aiagaru@stanford.edu
Published online Dec. 10, 2015.

outside the expected physiologic biodistribution with that of ^{68}Ga-RM2 in the same patients.

MATERIALS AND METHODS

Patient Population

The local Radioactive Drug Research Committee, the local Institutional Review Board, and the Stanford Cancer Institute Scientific Review Committee approved the protocol. Written informed consent was obtained from all patients before they participated in the study. Inclusion criteria were age greater than 18 y at the time of radiotracer administration, a known diagnosis of prostate cancer, suspected recurrence based on biochemical data (PSA > 2 ng/mL), and ability to remain still during the imaging procedure (~1 h). Exclusion criteria were metallic/conductive or electrically/magnetically active implants without MR-safe or MR-conditional labeling and standard contraindications to PET and MRI per the screening policy of our hospital (e.g., severe claustrophobia or radiation phobia).

Preparation of ^{68}Ga-PSMA-11

^{68}Ga-PSMA-11 was synthesized as previously reported (*21*). The precursor, Glu-NH-CO-NH-Lys(Ahx)-HBED-CC (DKFZ-PSMA-11, or PSMA-HBED), was obtained from ABX GmbH. All other reagents were of the highest grade, were purchased from a commercial supplier (Sigma, EMD Millipore), and were used as provided.

The radiosynthesis was performed on a fully automated device using sterile single-use cassettes (Modular Lab PharmTracer; Eckert & Ziegler Eurotope GmbH). $^{68}GaCl_3$ was obtained from a ^{68}Ge/^{68}Ga generator (IGG-100 [1,850 MBq]; Eckert & Ziegler Isotope Products) by eluting the generator with 6 mL of 0.1 M HCl. The generator eluate was passed through a strong-cation-exchange cartridge to trap the ^{68}Ga ions for purification. Purified $^{68}GaCl_3$ was eluted from the cartridge using a concentrated NaCl/HCl solution into a precharged reaction vial containing the precursor DKFZ-PSMA-11 (10 μg) in sodium acetate buffer (pH 4.5). The mixture was heated at 85°C for 180 s. Crude ^{68}Ga-PSMA-11 was diluted with saline and loaded onto a C18 light cartridge. The loaded cartridge was subsequently washed with saline and eluted with a 50% ethanol solution. The purified product was then diluted with saline and passed through a sterilizing membrane filter (0.2 μm) to afford the final formulated product (~10 mL).

The identity and radiochemical purity of the product (^{68}Ga-PSMA-11) were evaluated by radio–high-performance liquid chromatography and radio–thin-layer chromatography. Estimated decay-corrected yield to the start of synthesis was 86.5% ± 4.1%, with a specific radioactivity of 70 ± 20 GBq/μmol (n = 10).

Preparation of ^{68}Ga-RM2

The precursor of ^{68}Ga-RM2, DOTA-4-amino-1-carboxymethylpiperidine-D-Phe-Gln-Trp-Ala-Val-Gly-His-Sta-Leu-NH_2 (DOTA-RM2), was obtained from ABX GmbH. A ^{68}Ga-labeling kit including eluent (concentrated NaCl/HCl solution), sodium acetate reaction buffer, ethanol (50% in water), and saline (0.9%, U.S. Pharmacopeia) was obtained from Eckert & Ziegler Eurotope GmbH. Phosphate buffer concentrate (1 M Na^+, 0.6 M PO_4^{3-}) for pH adjustment was obtained from B. Braun.

Purified $^{68}GaCl_3$ was eluted from the strong-cation-exchange cartridge using a concentrated NaCl/HCl solution into a precharged reaction vial containing the precursor DOTA-RM2 (40 μg) in sodium acetate buffer (pH 4.5) and ethanol. The mixture was heated at 105°C for 400 s. Crude ^{68}Ga-RM2 was diluted with phosphate-buffered saline and loaded onto a C18 light cartridge. The loaded cartridge was subsequently washed with buffered saline and eluted with a 50% ethanol solution. The purified product was then diluted with phosphate-buffered saline and passed through a sterilizing membrane filter (0.2 μm) to afford the final formulated product (~10 mL).

The identity and radiochemical purity of the product (^{68}Ga-RM2) were evaluated by radio–high-performance liquid chromatography and radio–thin-layer chromatography. Estimated decay-corrected yield to the start of synthesis was 86.1% ± 1.2%, with a specific radioactivity of 16 ± 1 GBq/μmol (n = 7).

PET/CT Protocol

No specific patient preparation such as fasting or hydration was requested for ^{68}Ga-PSMA-11 PET/CT scans. Whole-body PET/CT images were acquired from vertex to mid thighs with 8 bed positions and 3-min emission scans per bed position at 51–68 min (mean ± SD, 57.1 ± 5.9 min) after intravenous administration of the ^{68}Ga-PSMA-11. The administered activity was 130–144 MBq (mean ± SD, 137 ± 4 MBq). The images were reconstructed using an ordered-subset expectation maximization algorithm with 2 iterations and 32 subsets for the Discovery 600 scanner (GE Healthcare) (6 patients) and 2 iterations and 24 subsets for the Discovery 690 scanner (GE Healthcare) (1 patient). The CT acquisition was performed for attenuation correction, in helical mode, using 120 kV, 10 mAs, a 512 × 512 matrix, and an 867-mm field of view in 22.5 s. The CT amperage was reduced to 10 mAs, as requested by the local Institutional Review Board, to decrease the radiation exposure. The duration of the PET/CT examination ranged from 24 to 38 min (mean ± SD, 30.2 ± 4.9 min).

PET/MRI Protocol

No specific patient preparation such as fasting or hydration was required on the day of the ^{68}Ga-RM2 PET/MRI scans. Imaging (vertex to mid thighs) started at 42–51 min (mean ± SD, 48 ± 3 min) after injection of 133–152 MBq (mean ± SD, 137 ± 7 MBq) of ^{68}Ga-RM2 using a time-of-flight–enabled simultaneous PET/MRI scanner (Signa; GE Healthcare). The duration of the scan ranged from 39 to 85 min (mean ± SD, 66 ± 16 min) and, in addition to the difference in number of bed positions used related to patient height, also included the time to prepare the patients for the scans (e.g., positioning the body coils and defining the field of view). Lastly, patients who had not undergone prostatectomy received intravenous contrast material and underwent additional T1-weighted imaging over the prostate bed, contributing to the duration of the examination. The PET acquisition was performed in 3-dimensional mode at 4 min per bed position (89 slices per bed position) in 5–9 bed positions. An axial 2-point Dixon 3-dimensional T1-weighted spoiled gradient echo MR sequence (repetition time/first echo time/second echo time, 4.1/1.1/2.2 ms; field of view, 50 × 37.5 cm; matrix, 256 × 128; slice thickness/spacing, 5.2/2.6 mm; 120 images per slab; imaging time, 18 s) was acquired at each bed position and used to generate attenuation correction maps and to allow anatomic registration of the PET results.

PET images were reconstructed using ordered-subsets expectation maximization with 2 iterations and 28 subsets. Time-of-flight reconstructed images assumed a gaussian kernel of 400-ps width. The Dixon MRI sequence and the PET acquisition started at the same bed position and times, thus ensuring optimal temporal and regional correspondence between the MRI and PET data. For attenuation correction, the images were segmented into different tissue types with an anatomy-aware algorithm and were coregistered to a CT atlas in the head region (*22*).

Additional sequences acquired at each station included coronal T2-weighted single-shot fast spin echo imaging, diffusion-weighted imaging, and T1-weighted axial 2-point Dixon 3-dimensional spoiled gradient echo imaging, as previously described (*22*).

Image Analysis

Two board-certified nuclear medicine physicians with 10 and 8 y of experience in interpreting PET studies used MIMvista (version 6.2;

TABLE 1
Patient Characteristics and Scan Results

Patient no.	Age (y)	Initial cancer stage	Gleason score	PSA (ng/mL)	Treatment	^{68}Ga-PSMA-11	^{68}Ga-RM2
1	83	II	5 + 4	16.2	HT + IMRT	Retroperitoneal LNs	Retroperitoneal LNs
2	69	II	3 + 4	6.0	Prostatectomy	Retroperitoneal LNs	Retroperitoneal LNs
3	75	IV	4 + 5	36.5	Prostatectomy	Retroperitoneal LNs, pelvic LN	Retroperitoneal LNs, pelvic LN
4	67	III	3 + 3	6.7	Brachytherapy + HT	Vas deferens, pelvic LN	Negative
5	72	III	4 + 3	3.5	RT	Supraclavicular LN	Supraclavicular LN
6	81	I	3 + 4	7.4	Prostatectomy	Pelvic LNs, seminal vesicle	Pelvic LNs, seminal vesicle
7	73	III	4 + 4	18.2	Prostatectomy	Mediastinal LNs, retroperitoneal LNs, pelvic LNs, multiple bone lesions	Mediastinal LNs, retroperitoneal LNs, pelvic LNs, multiple bone lesions

HT = hormone therapy; IMRT = intensity-modulated radiation therapy; LN = lymph node; RT = radiation therapy.

MIMvista Corp.) to select organs throughout the body and used the region-of-interest (ROI) tool within the software to evaluate uptake. Circular ROIs, whose sizes (diameter, 10–30 mm) depended on the structure of interest, were drawn on transaxial ^{68}Ga-RM2 PET/MR images and transaxial ^{68}Ga-PSMA-11 PET/CT images with reference to anatomic structures confirmed by the MRI portion of the PET/MRI scan and the CT portion of the PET/CT scan, respectively. ROIs were analyzed for the frontal lobe cortex, cerebellar cortex, parotid gland, submandibular gland, thyroid, lung, ascending aorta as blood pool, liver, spleen, pancreas, small intestine, descending colon, kidney, bladder, gluteus maximus muscle, fat tissue of hip, right humerus, right femur, third cervical vertebra, ninth thoracic vertebra, third lumbar vertebra, and sacrum. To account for specific biodistribution, we added ROI measurements for esophagus and stomach for ^{68}Ga-RM2 and lacrimal grand and submandibular salivary gland for ^{68}Ga-PSMA-11. These ROIs were carefully positioned over the central portion of each structure depicted on the PET/MR or PET/CT image. For the aortic blood pool, a circular 10-mm-diamter ROI was placed centrally within the ascending aorta. A 30-mm-diameter ROI was placed on the right liver lobe.

For SUV measurements of focal ^{68}Ga-RM2 uptake outside the expected biodistribution, we reviewed the PET images with reference to the MRI data. Conversely, for SUV measurements of focal ^{68}Ga-PSMA-11 uptake outside the expected biodistribution, we reviewed the PET images with reference to the CT data. The PETedge tool of MIMvista was used to measure ^{68}Ga-RM2 and ^{68}Ga-PSMA-11 uptake outside the expected biodistribution.

Two board-certified radiologists (9 and 2 y of experience in interpreting body MRI studies) who did not know the results of PET or other studies evaluated the MR images for areas of abnormal signal or anatomic structures. Visual conspicuity against background on the diffusion-weighted images and presence of an anatomically corresponding abnormality on the T1- and T2-weighted images were the criteria for detecting a lesion on MRI.

Statistical Analysis

Data on time from injection to start of imaging, injected dosages of radiopharmaceuticals, SUV_{mean}, and SUV_{max} are presented as mean ± SD. The Mann–Whitney *U* test was used to evaluate focal uptake outside the expected biodistribution between ^{68}Ga-RM2 and ^{68}Ga-PSMA-11 (SUV_{mean}, SUV_{max}, and F/N ratio [ratio of SUV_{mean} and SUV_{max} to normal background, i.e., blood pool). The Pearson correlation coefficient was used to evaluate ^{68}Ga-RM2 and ^{68}Ga-PSMA-11 uptake. All statistical analyses were done with Stata 11 (Stata). Two-tailed *P* values of less than 0.05 were considered significant.

RESULTS

Seven men (67–83 y old; mean ± SD, 74.3 ± 5.9 y) with suspected biochemical recurrence of prostate cancer and PSA levels of 13.5 ± 11.5 ng/mL (range, 3.5–36.5 ng/mL) were enrolled in this

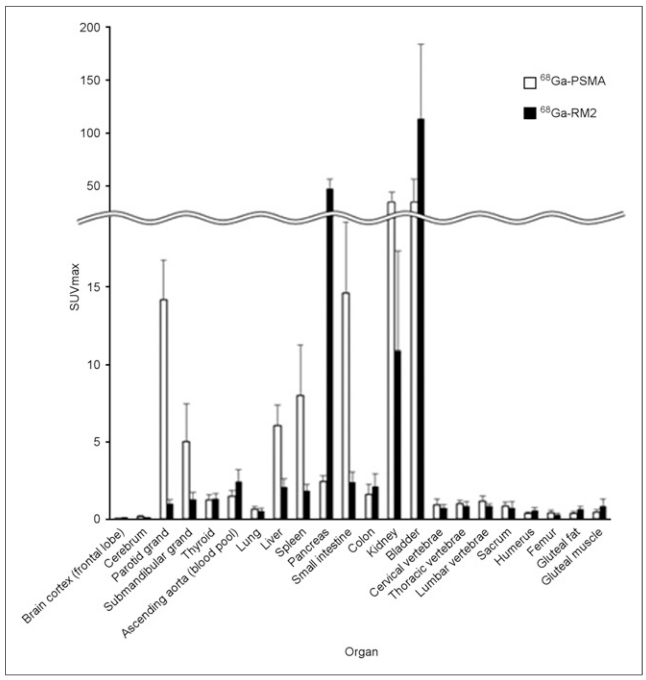

FIGURE 1. SUV_{max} of ^{68}Ga-PSMA-11 and ^{68}Ga-RM2 images for all analyzed normal tissues.

TABLE 2
^{68}Ga-PSMA-11 and ^{68}Ga-RM2 Uptake Outside Expected Physiologic Biodistribution

Index	^{68}Ga-PSMA-11	^{68}Ga-RM2	*P*
SUV_{max}	12.4 ± 7.1 (4.1–43.6)	13.2 ± 8.0 (2.5–33.5)	0.63
SUV_{mean}	7.1 ± 4.0 (2.0–14.4)	7.6 ± 3.8 (2.0–14.4)	0.38
F/N ratio	10.4 ± 9.3 (2.3–42.8)	5.9 ± 4.6 (1.2–18.8)	<0.003
F/N ratio	9.2 ± 7.3 (2.4–40.4)	5.2 ± 3.5 (1.6–12.8)	<0.02

Data are mean ± SD, followed by range in parentheses.

study. Patient characteristics and results are shown in Table 1. The patients underwent standard-of-care imaging studies (CT, MRI, ^{18}F-FDG PET/CT, ^{18}F-NaF PET/CT, or ^{99m}Tc-MDP bone scanning) before enrollment that had noncontributory results. ^{68}Ga-RM2 PET/MRI was performed first, followed by ^{68}Ga-PSMA-11 PET/CT 13–85 d later (mean ± SD, 42.9 ± 25.2 d later). The time from conventional imaging to ^{68}Ga-RM2 PET/MRI was 10–107 d (mean ± SD, 43.3 ± 26.0 d). The interval from biochemical recurrence to the ^{68}Ga-RM2 PET/MRI scan was 5–75 mo (mean ± SD, 30.8 ± 20.4 mo). The interval from the most recent PSA measurement to the ^{68}Ga-RM2 PET/MRI scan was 1–30 d (mean ± SD, 15.2 ± 12.2 d).

Biodistribution and Localization of ^{68}Ga-PSMA-11 and ^{68}Ga-RM2

All patients were on a watch-and-wait management strategy at the time of enrollment. All tolerated the procedure without immediate or delayed (≤7 d) reportable adverse events.

The tissues with the highest uptake of ^{68}Ga-PSMA-11 were lacrimal, parotid, and submandibular glands and small intestine, whereas those with the highest ^{68}Ga-RM2 accumulation were pancreas and bladder (Fig. 1; Supplemental Table 1 [supplemental materials are available at http://jnm.snmjournals.org]).

^{68}Ga-PSMA-11 and ^{68}Ga-RM2 Uptake Outside the Expected Physiologic Biodistribution

There were 45 areas of high ^{68}Ga-PSMA-11 uptake. These corresponded on the CT images to bone marrow (n = 13), retroperitoneal lymph nodes (n = 12), mediastinal lymph nodes (n = 8), pelvic lymph nodes (n = 9), seminal vesicle (n = 2), and subclavian lymph node (n = 1). ^{68}Ga-RM2 uptake was high in all these areas with two exceptions: a pelvic lymph node and vas deferens that were negative on the ^{68}Ga-RM2 study, both in the same patient. The time from ^{68}Ga-RM2 to ^{68}Ga-PSMA-11 was 54 d in this patient, with PSA changing from 6.8 to 9.2 ng/mL during the interval. Conversely, in two patients ^{68}Ga-PSMA-11 uptake or clearance in the bowel made small retroperitoneal lymph nodes less conspicuous on ^{68}Ga-PSMA-11 images than on ^{68}Ga-RM2 images.

^{68}Ga-PSMA-11 uptake outside the expected physiologic biodistribution was not statistically significant when compared with ^{68}Ga-RM2 uptake in the same areas (P = 0.63 for SUV_{max} and 0.38 for SUV_{mean}; Table 2). The correlation coefficients between uptake of the two tracers were 0.62 ($P < 0.001$) for SUV_{max} and 0.54 ($P < 0.001$) for SUV_{mean}.

The F/N ratios for ^{68}Ga-PSMA-11 were statistically higher than those for ^{68}Ga-RM2 (F/N ratio by SUV_{max}, 5.9 ± 4.6, $P < 0.003$; F/N ratio by SUV_{mean}, 5.2 ± 3.5, $P < 0.02$) (Table 2). Representative images are shown in Figures 2–4 and Supplemental Figures 1 and 2. Data from clinical follow-up are shown in Table 3.

DISCUSSION

In the present study, ^{68}Ga-PSMA-11 showed high accumulation in the lacrimal glands, parotid glands, submandibular glands, small intestine, kidneys, and bladder, and ^{68}Ga-RM2 showed high accumulation in the pancreas and bladder. To our knowledge, this was the first study directly comparing the biodistribution of these PET tracers in normal tissues and outside the expected physiologic biodistribution in patients with biochemically recurrent prostate cancer. The fact that ^{68}Ga-PSMA-11 has both renal and hepatobiliary clearance whereas ^{68}Ga-RM2 has mainly renal clearance may have implications for the detection of abdominal and pelvic lesions, as bowel uptake or clearance may mask small lesions. ^{68}Ga-PSMA-11 and ^{68}Ga-RM2 had a similar localization in lymph nodes, seminal vesicles, and bone marrow, but the slower clearance of ^{68}Ga-RM2 from the major-vessel blood pool resulted in less conspicuous uptake in the mediastinal and supraclavicular lymph nodes. Conversely, ^{68}Ga-PSMA-11 uptake or clearance in the bowel made small retroperitoneal lymph nodes less conspicuous on ^{68}Ga-PSMA-11 imaging than on ^{68}Ga-RM2 imaging in two patients. There was only one patient in whom ^{68}Ga-RM2 imaging was negative for uptake but ^{68}Ga-PSMA-11 imaging was not, showing focal uptake in 1 pelvic lymph node and seminal vesicle. But in this patient the two scans were obtained 54 d apart.

Previous work showed PSMA receptor expression to be in the kidneys and spleen, whereas gastrin-releasing peptide receptor expression was primarily in the pancreas (*23*). Our results are consistent with the uptake pattern that was previously reported for both ^{68}Ga-RM2 and ^{68}Ga-PSMA-11 (*16,24*). ^{68}Ga-RM2 and

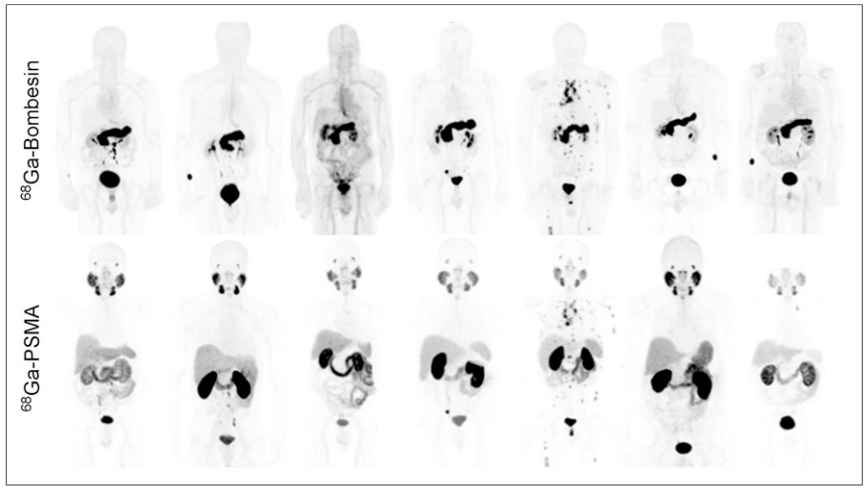

FIGURE 2. Maximum-intensity-projection ^{68}Ga-RM2 and ^{68}Ga-PSMA-11 images of the 7 enrolled patients.

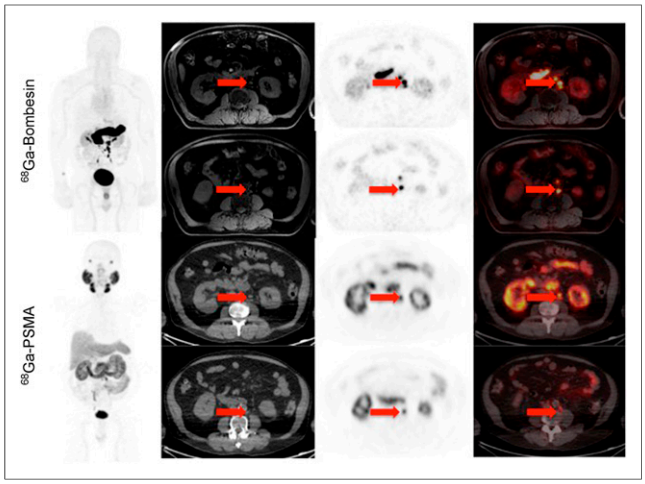

FIGURE 3. 83-y-old man with history of Gleason 5 + 4 prostate cancer treated with radiation therapy and androgen blockade, who presented with PSA level of 18.7 ng/mL and noncontributory findings on conventional imaging. Maximum-intensity-projection ^{68}Ga-RM2 and ^{68}Ga-PSMA-11 images, as well as axial PET images, show subcentimeter focal uptake corresponding to lymph nodes on MRI and CT, respectively.

^{68}Ga-PSMA-11 target different biologic processes; therefore, understanding how these tracers behave in patients with biochemically recurrent prostate cancer is critical to finding the best management options for this clinical scenario, as neither is expected to be 100% sensitive or specific. We expect that certain patients will benefit from having both scans done.

The first large study of ^{68}Ga-PSMA-11 in patients with prostate cancer showed that it could detect recurrent prostate cancer with high specificity in a large proportion of patients (*25*). The detection rates of ^{68}Ga-PSMA-11 for recurrent disease were 96.8% when PSA levels were at least 2 ng/mL and 57.9% for PSA levels of between 0.2 and less than 0.5 ng/mL in a study evaluating 248

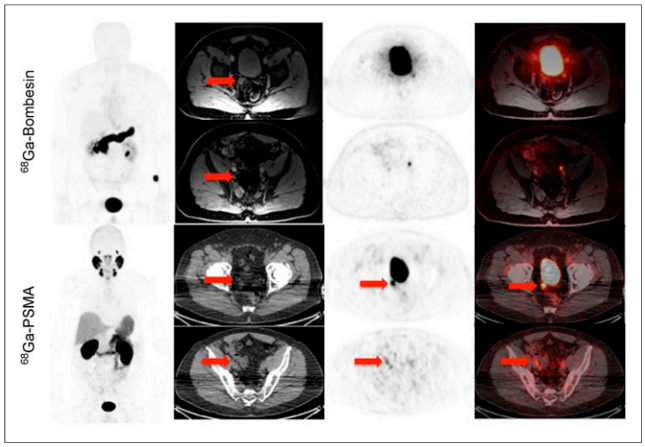

FIGURE 4. 67-y-old man with history of Gleason 3 + 3 prostate cancer treated with radiation therapy and androgen blockade, who presented with PSA level of 6.7 ng/mL and noncontributory findings on conventional imaging. ^{68}Ga-RM2 images are negative for uptake, whereas maximum-intensity-projection ^{68}Ga-PSMA-11 images, as well as axial PET images, show subcentimeter focal uptake corresponding to pelvic lymph node and right seminal vesicle on CT. These were biopsy-proven to represent metastatic disease.

TABLE 3
Follow-up Results After Scanning

Patient no.	Follow-up results
1	Started bicalutamide and leuprolide, and PSA decreased from 18.7 to 2.53; follow-up MRI showed decreased size and number of retroperitoneal lymph nodes
2	Chose to have no treatment, and PSA increased from 8.6 to 10.9
3	Started bicalutamide and leuprolide, and PSA decreased from 36.4 to 2.2
4	Started no treatment yet, and PSA increased from 6.7 to 12.1; on biopsy, 12 prostate cores were negative and right vas deferens showed metastatic adenocarcinoma (Gleason 4 + 3; 15% of core)
5	Started no treatment yet, and PSA increased from 8.53 to 10.2
6	Started bicalutamide, and PSA decreased from 7.36 to 0.38
7	Started bicalutamide, and PSA decreased from 18.2 to 2.5

patients with biochemical recurrence after radical prostatectomy. The detection rates increased with higher Gleason scores and were not influenced by antiandrogen therapy (*26*). Several studies showed ^{68}Ga-PSMA-11 PET/CT to perform better than ^{18}F-choline (*27,28*).

The sensitivity of ^{68}Ga-RM2 in a subsector analysis of whole prostatectomy samples was 88% for the detection of primary prostate cancer and 70% for the detection of lymph node metastases (*29*). Early work indicated that gastrin-releasing peptide receptors are expressed primarily in early and androgen-dependent prostate tumors; however, others have reported high expression of gastrin-releasing peptide receptors in metastatic disease as well (*30*). ^{68}Ga-RM2 targets gastrin-releasing peptide receptors and therefore appears to have potential for detecting prostate cancer lesions, which generally grow slowly and are difficult to detect with conventional imaging in the biochemical recurrence scenario. Our study showed similar, but not identical, uptake patterns for ^{68}Ga-RM2 and ^{68}Ga-PSMA-11 in suspected lesions. This difference may be due to heterogeneous expression of PSMA and gastrin-releasing peptide receptors or to a partial loss of expression of either of these receptors.

One limitation of our study was the small number of patients, but this is common for pilot studies done under Radioactive Drug Research Committee approval. Another limitation was the lack of correlation with pathology results for all patients. Only basic information on biodistribution and radiopharmaceutical localization could be collected, because the Radioactive Drug Research Committee mechanism does not allow data collection for immediate therapeutic, diagnostic, or similar purposes or to determine the safety and effectiveness of a radioactive drug in humans. However, given the encouraging preliminary results of this pilot study, we plan to evaluate ^{68}Ga-PSMA-11 and ^{68}Ga-RM2 further in a

larger cohort of patients with biochemically recurrent prostate cancer, including patients with a PSA level of 0.5 ng/mL or higher. Lastly, because of the funding resources, the patients were imaged with PET/MRI for ^{68}Ga-RM2 studies and PET/CT for ^{68}Ga-PSMA-11 studies. This may be seen as a bias toward ^{68}Ga-RM2, given the superior detectors and image quality of the PET/MRI scanner (*22*).

CONCLUSION

The a priori expectation from previous studies was that ^{68}Ga-PSMA-11 would perform much better than ^{68}Ga-RM-2 in a cohort of patients with biochemically recurrent prostate cancer. The findings indicate that additional work is needed to understand the expression of PSMA and gastrin-releasing peptide receptors in different types of prostate cancer. One may therefore imagine personalizing biomarker assessments in the future for patients with prostate cancer. This study also highlights the significant advances in ^{68}Ga-labeled PET tracers in recent years and the need for consistent regulatory policies to allow easy access to such important radiotracers, including ^{68}Ga-RM2.

ACKNOWLEDGMENTS

This study is registered on Clinicaltrials.gov as NCT02440308 (^{68}Ga-RM2) and NCT02488070 (^{68}Ga-PSMA-11). We thank Dawn Banghart, George Segall, and the other members of the Radioactive Drug Research Committee for advice and support; Zhen Cheng and Xiaowei Ma for assistance with implementing the ^{68}Ga-PSMA-11 synthesis; Mathias Berndt, Andre Mueller, and Andrew Stephens (Piramal Imaging, GmbH) for assistance with preparing ^{68}Ga-RM2; Markus Schwaiger (TUM) and Klaus Kopka (DKFZ Heidelberg) for assistance with preparing ^{68}Ga-PSMA-11; and Ali Afshar-Oromieh (University Hospital Heidelberg) for assistance with the ^{68}Ga-PSMA-11 dosimetry data. We also thank our research coordinators, Pam Gallant and Krithika Rupnarayan; the Stanford Cyclotron and Radiochemistry Facility; and the nuclear medicine technologists. We especially thank all the patients who agreed to participate in the study and their families.

REFERENCES

1. D'Amico AV, Whittington R, Malkowicz SB, et al. Pretreatment nomogram for prostate-specific antigen recurrence after radical prostatectomy or external-beam radiation therapy for clinically localized prostate cancer. *J Clin Oncol.* 1999; 17:168–172.
2. Hanlon AL, Moore DF, Hanks GE. Modeling postradiation prostate specific antigen level kinetics: predictors of rising postnadir slope suggest cure in men who remain biochemically free of prostate carcinoma. *Cancer.* 1998;83: 130–134.
3. Kelloff GJ, Choyke P, Coffey DS. Challenges in clinical prostate cancer: role of imaging. *AJR.* 2009;192:1455–1470.
4. Oyama N, Miller TR, Dehdashti F, et al. ^{11}C-acetate PET imaging of prostate cancer: detection of recurrent disease at PSA relapse. *J Nucl Med.* 2003;44: 549–555.
5. Picchio M, Messa C, Landoni C, et al. Value of [^{11}C]choline-positron emission tomography for re-staging prostate cancer: a comparison with [^{18}F]fluorodeoxyglucose-positron emission tomography. *J Urol.* 2003;169:1337–1340.
6. Albrecht S, Buchegger F, Soloviev D, et al. ^{11}C-acetate PET in the early evaluation of prostate cancer recurrence. *Eur J Nucl Med Mol Imaging.* 2007;34: 185–196.
7. Wachter S, Tomek S, Kurtaran A, et al. ^{11}C-acetate positron emission tomography imaging and image fusion with computed tomography and magnetic resonance imaging in patients with recurrent prostate cancer. *J Clin Oncol.* 2006;24:2513–2519.
8. Beheshti M, Haim S, Zakavi R, et al. Impact of ^{18}F-choline PET/CT in prostate cancer patients with biochemical recurrence: influence of androgen deprivation therapy and correlation with PSA kinetics. *J Nucl Med.* 2013;54:833–840.
9. Heinisch M, Dirisamer A, Loidl W, et al. Positron emission tomography/computed tomography with F-18-fluorocholine for restaging of prostate cancer patients: meaningful at PSA < 5 ng/ml? *Mol Imaging Biol.* 2006;8:43–48.
10. Vees H, Buchegger F, Albrecht S, et al. ^{18}F-choline and/or ^{11}C-acetate positron emission tomography: detection of residual or progressive subclinical disease at very low prostate-specific antigen values (<1 ng/mL) after radical prostatectomy. *BJU Int.* 2007;99:1415–1420.
11. Sweat SD, Pacelli A, Murphy GP, Bostwick DG. Prostate-specific membrane antigen expression is greatest in prostate adenocarcinoma and lymph node metastases. *Urology.* 1998;52:637–640.
12. Eder M, Eisenhut M, Babich J, Haberkorn U. PSMA as a target for radiolabelled small molecules. *Eur J Nucl Med Mol Imaging.* 2013;40:819–823.
13. Zechmann C, Afshar-Oromieh A, Armor T, et al. Radiation dosimetry and first therapy results with a ^{124}I/^{131}I-labeled small molecule (MIP-1095) targeting PSMA for prostate cancer therapy. *Eur J Nucl Med Mol Imaging.* 2014;41:1280–1292.
14. Weineisen M, Schottelius M, Simecek J, et al. ^{68}Ga- and ^{177}Lu-Labeled PSMA I&T: optimization of a PSMA-targeted theranostic concept and first proof-of-concept human studies. *J Nucl Med.* 2015;56:1169–1176.
15. Ahmadzadehfar H, Rahbar K, Kurpig S, et al. Early side effects and first results of radioligand therapy with ^{177}Lu-DKFZ-617 PSMA of castrate-resistant metastatic prostate cancer: a two-centre study. *EJNMMI Res.* 2015;5:114.
16. Afshar-Oromieh A, Malcher A, Eder M, et al. PET imaging with a [^{68}Ga]gallium-labelled PSMA ligand for the diagnosis of prostate cancer: biodistribution in humans and first evaluation of tumour lesions. *Eur J Nucl Med Mol Imaging.* 2013;40:486–495.
17. Jensen RT, Battey JF, Spindel ER, Benya RV. International Union of Pharmacology. LXVIII. Mammalian bombesin receptors: nomenclature, distribution, pharmacology, signaling, and functions in normal and disease states. *Pharmacol Rev.* 2008;60:1–42.
18. Reubi JC, Wenger S, Schmuckli-Maurer J, Schaer J-C, Gugger M. Bombesin receptor subtypes in human cancers: detection with the universal radioligand ^{125}I-[d-TYR6, β-ALA11, PHE13, NLE14] bombesin(6–14). *Clin Cancer Res.* 2002;8:1139–1146.
19. Sun B, Halmos G, Schally AV, Wang X, Martinez M. Presence of receptors for bombesin/gastrin-releasing peptide and mRNA for three receptor subtypes in human prostate cancers. *Prostate.* 2000;42:295–303.
20. Markwalder R, Reubi JC. Gastrin-releasing peptide receptors in the human prostate: relation to neoplastic transformation. *Cancer Res.* 1999;59:1152–1159.
21. Eder M, Neels O, Muller M, et al. Novel preclinical and radiopharmaceutical aspects of [^{68}Ga]Ga-PSMA-HBED-CC: a new PET tracer for imaging of prostate cancer. *Pharmaceuticals (Basel).* 2014;7:779–796.
22. Iagaru A, Mittra E, Minamimoto R, et al. Simultaneous whole-body time-of-flight ^{18}F-FDG PET/MRI: a pilot study comparing SUVmax with PET/CT and assessment of MR image quality. *Clin Nucl Med.* 2015;40:1–8.
23. Eder M, Schafer M, Bauder-Wust U, Haberkorn U, Eisenhut M, Kopka K. Preclinical evaluation of a bispecific low-molecular heterodimer targeting both PSMA and GRPR for improved PET imaging and therapy of prostate cancer. *Prostate.* 2014;74:659–668.
24. Roivainen A, Kahkonen E, Luoto P, et al. Plasma pharmacokinetics, whole-body distribution, metabolism, and radiation dosimetry of ^{68}Ga bombesin antagonist BAY 86-7548 in healthy men. *J Nucl Med.* 2013;54:867–872.
25. Afshar-Oromieh A, Avtzi E, Giesel F, et al. The diagnostic value of PET/CT imaging with the ^{68}Ga-labelled PSMA ligand HBED-CC in the diagnosis of recurrent prostate cancer. *Eur J Nucl Med Mol Imaging.* 2015;42:197–209.
26. Eiber M, Maurer T, Souvatzoglou M, et al. Evaluation of hybrid ^{68}Ga-PSMA ligand PET/CT in 248 patients with biochemical recurrence after radical prostatectomy. *J Nucl Med.* 2015;56:668–674.
27. Morigi JJ, Stricker PD, van Leeuwen PJ, et al. Prospective comparison of ^{18}F-fluoromethylcholine versus ^{68}Ga-PSMA PET/CT in prostate cancer patients who have rising PSA after curative treatment and are being considered for targeted therapy. *J Nucl Med.* 2015;56:1185–1190.
28. Afshar-Oromieh A, Zechmann CM, Malcher A, et al. Comparison of PET imaging with a ^{68}Ga-labelled PSMA ligand and ^{18}F-choline-based PET/CT for the diagnosis of recurrent prostate cancer. *Eur J Nucl Med Mol Imaging.* 2014;41:11–20.
29. Kähkönen E, Jambor I, Kemppainen J, et al. In vivo imaging of prostate cancer using [^{68}Ga]-labeled bombesin analog BAY86-7548. *Clin Cancer Res.* 2013;19:5434–5443.
30. de Visser M, van Weerden WM, de Ridder CM, et al. Androgen-dependent expression of the gastrin-releasing peptide receptor in human prostate tumor xenografts. *J Nucl Med.* 2007;48:88–93.